PHARMACIA

Pharmacia 68(1): 201–209
DOI 10.3897/pharmacia.68.e60685

Research Article

Rosemary oil nano-emulsion potentiates the apoptotic effect of mitomycin C on cancer cells *in vitro*

Waad Al-otaibi[1]

1 *Chemistry Department, College of Science and Humanities, Shaqra University, Al-Dawadmi, Saudi Arabia*

Corresponding author: Waad Al-otaibi (w.otaibi@su.edu.sa)

Received 12 November 2020 ♦ **Accepted** 9 January 2021 ♦ **Published** 9 February 2021

Citation: Al-otaibi W (2021) Rosemary oil nano-emulsion potentiates the apoptotic effect of mitomycin C on cancer cells *in vitro*. Pharmacia 68(1): 201–209. https://doi.org/10.3897/pharmacia.68.e60685

Abstract

Purpose: To formulate nano-emulsified rosemary oil (REO/NE) and determine its effect on the anticancer agent, mitomycin C (MC) when used as a carrier for the drug.

Methods: The droplet size of REO/NE was markedly enlarged when mixed with MC. The cytotoxicity of the formulations on HeLa and MCF-7 cells was determined using MTT assay. The combination index (CI) values were estimated with CompuSyn software, while apoptosis was determined using DAPI fluorescent dye.

Results: Treatment of MCF-7 cells and HeLa cells with REO/NE (1% v:v and 1.33% v:v, respectively) reduced the IC_{50} of MC 33 and 15 folds, respectively. Under fluorescent microscopy, cells treated with REO/NE+MC had more marked reduction of the nuclear area than MC-treated cells.

Conclusion: These results indicate that REO/NE is an efficient carrier for MC since it enhanced MC delivery and increased its effect on the cells through the induction of apoptosis at low concentrations of MC.

Keywords

Rosemary oil nano-emulsion, Mitomycin C, Synergy, Apoptosis, Anticancer effect

Introduction

Mitomycin C (MC) is an antineoplastic and antibiotic agent that exerts antitumor activity and apoptosis through inhibition of DNA synthesis by forming covalent cross-linkages with guanine in the DNA minor groove region. However, the clinical uses and efficacy of MC are extensively limited on account of its toxicity in normal cells (Ozerhan et al. 2016; Urkan et al. 2017). Combination chemotherapy has been extensively used, and it is considered as one of the promising strategies for combating several types of cancer (Alkhatib et al. 2018; AlMotwaa et al. 2020). It has advantages in that the multiple drug therapy targets multiple signal transduction pathways in cancer cells, while a single chemotherapeutic agent is utilized as an inhibitor for only one signal transduction route. In order to reduce the doses of chemotherapeutics and enhance their cytotoxic effects, MC has been combined with other compounds such as vanillic acid (Erdem et al. 2012); doxorubicin (Kostková et al. 2013); curcumin (Zhou et al. 2015); astaxanthin (Ko et al. 2016); 5-fluorouracil (Murata et al. 2018), and cisplatin (Pinto and Pocard 2019). However, combination treatments are frequently affected by the different pharmacokinetic pro-

files from the different physicochemical properties of the combined drugs (Jo et al. 2020). These problems may be solved using nano-delivery systems due to their ability to encapsulate various types of drugs and to synergize their pharmacokinetic properties (Arpagaus 2019; Elmowafy et al. 2019). Nano-emulsion (NE) systems have specific features that make them quite attractive as promising nano-delivery systems (Karami et al. 2019; Chevalier and Bolzinger 2019; AlMotwaa et al. 2020; Al-Otaibi et al.). They are colloidal dispersions composed of an oil phase, an aqueous phase and a mixture of surfactant and co-surfactant with droplet diameters typically in the range of 10 to 100 nm (Sutradhar and Amin 2013). Nano-emulsion (NE) systems containing essential oils have been shown to have stronger antimicrobial effects both *in vivo* and *in vitro*, when compared to essential oil either in the free or in coarse emulsion forms (Guo et al. 2020).

Rosemary oil (REO) has marked antioxidant, chemo-preventive, anti-proliferative and cytotoxic properties (Ahamad et al. 2019; Chraibi et al. 2020; Bouyahya et al. 2020; Wang et al. 2012; Rašković et al. 2014; Sujatha and Sirisha 2019). Gezici et al. (2017) reported that REO produced strong inhibitory effect on the proliferation of different cancer cell lines: human lung adenocarcinoma (A549), human non-small lung cancer (H1299), and human breast adenocarcinoma (MCF-7), with IC_{50} values ranging from 3.06 to 7.38 µg/ml. The anticancer effect of REO on MCF-7 cells was improved when administered in form of a liposomal system, relative to free REO (Salari and Salari 2019). In another study, it was reported that at high concentrations, REO induced apoptosis signaling pathways, DNA fragmentation and arrest of hepatoma (HepG2) cells in the G1 phase of the cell cycle (Melušová et al. 2014).

However, to date, there are no studies on the anticancer effects of REO-containing NE and the conventional anticancer agent. In the present work, an NE system containing REO and the conventional chemotherapeutic, MC, was produced using pressure homogenization technique (Liu et al. 2019), and the synergistic effect of the REO/NE on the anticancer activity of MC, on MCF-7 and HeLa cell lines was investigated.

Materials and methods

Chemical and cell cultures

All chemicals and reagents utilized in the study were obtained from Sigma-Aldrich (St. Louis, MO, USA). Mitomycin C (MC) was purchased from Korea United Pharma. Rosemary oil (REO) was obtained from Sukar Nabat for natural oil (Jeddah, KSA). Breast cancer (MCF-7) and Human cervical cancer (HeLa) cells were donated by the Tissue Culture Unit at King Fahad Center for Medical Research (Jeddah, KSA). Cancer cell lines were cultured in a 25-cm^2 cell culture flask in Dulbecco's modified Eagle's medium containing antibiotics (0.1 mg/mL penicillin, 100 U/mL streptomycin and 10% v/v) and fetal bovine serum and incubated at 37 °C in a 95% humidified atmosphere with 5% CO_2. The confluent cells were trypsinized using 0.2 ml of trypsin, and they were seeded in 24- or 96- well plates, based on the assay. The antineoplastic and apoptotic effects of the studied formulation against the cancer cells were measured using MTT assay and DAPI assay, respectively.

Production of REO/NE using high-pressure homogenization technique

Different weight fractions of oil phase (REO), hydrophilic phase (distilled water), and a mixture of surfactant and co-surfactant (tween 80 and span 20; 2:1 v:v) respectively, were mixed in Pyrex screw cap test tubes and heated up to 70 °C, with continuous mixing using a vortex mixer (VELP, Scientific, Italy) at 3000 rpm. This procedure was carried out to determine the best proportions of the constituents at which the one phase of REO/NE could be obtained. The resultant REO/NE was exposed to different temperatures (25 to 70 °C) to measure the opacity of the solution.

Preparation of REO/NE+MC

The REO/NE obtained was utilized as a carrier for MC. A stock solution of REO/NE+MC was produced by dissolving MC in REO/NE to yield solution of concentration 50 µg/ml of formula. Similarly, a 50 µg/ml stock solution of MC was prepared in normal saline (0.9% NaCl, w/v).

Determination of particle size and charge

The measurements of particle size, charge and polydispersity index for REO/NE and REO/NE+MC were carried out 25 ± 0.2 °C using Zetasizer (Malvern, Nano-ZS Worcestershire, UK). Three independent measurements for each sample were analyzed to obtain the parameters. The data are presented as mean ± SD ($\bar{x}$ ± SD).

Determination of cell growth inhibition with MTT assay

Assay of *in vitro* anticancer activity was conducted to determine the potential antiproliferative and cytotoxic properties of the combination formula, REO/NE+MC on the cancer cells. The MCF-7 and Hela cells were seeded in triplicate in 96-well culture plates, each at a density of 10×10^3cells/well and permitted to adhere for 24 h. Then, the cells were treated with different concentrations of REO/NE and MC for 24 h, to generate growth curves. The cells were incubated for 4 h with 0.5 ml of MTT solution (500 µg/ml) for 4 h 37 °C in the dark. Thereafter, the medium was discarded, and DMSO was added to the wells (0.1 ml/well) to dissolve the formazan crystals formed. The absorbance (Abs) of each well was recorded at 570 nm in a multiwell microplate reader (Bio Tek Instruments, Winooski, VT, USA). The Abs values were used to calculate percentage inhibition of cell growth, with the following equation:

$$\text{Growth inhibition (\%)} = 100 - \left(\frac{\text{Abs (treated cells)} - \text{Abs (blank)}}{\text{Abs(untreated cells)} - \text{Abs (blank)}} \times 100 \right)$$

Then, the data were transformed to the fraction affected (Fa) ranging from 0 to 1, where Fa=0 and Fa=1, representing 100 and 0% viability, respectively.

Determination of synergy

The results of MTT were input into Compusyn software (Biosoft, Ferguson, MO, USA) and utilized to estimate the values of combination index (CI) using the Chou-Talalay Method for non-constant ratio of combination. The effect of combinations, REO/NE + MC, was primarily reflected by the combination index CI, where CI< 1 indicates synergism, CI> 1 indicates antagonism, and CI=1 demonstrates an additive effect.

Assessment of nuclear morphology of apoptotic cells with DAPI staining

The MCF-7 and Hela cancer cells were grown overnight in 24-well plates at a density of 50×10^4 cells/well and treated for 24 h with three selected concentrations used in MTT assay of REO/NE, MC and the combined formula. Then, the cells were fixed with 4% paraformaldehyde solution in phosphate buffered saline (PBS, pH 7.4) for 30 min at room temperature, followed by rinsing with PBS for 5 min. The cells were permeabilized with Triton X-100 (0.1% in BPS) and stained using 4',6'-diamidino-2-phenylindole hydrochloride (DAPI) for 15 min in the dark. Finally, the images of morphological changes in the treated cells going through apoptosis were acquired using a fluorescence microscope (Leica CRT6000, Germany) with a blue filter at 437 µm. The mean nuclear area (in pixel^2) for each group was quantified using ImageJ analysis software (Rasband, W.S., ImageJ, National Institute of Health, US).

Statistical analysis

The analysis of data was performed with MegaStat version 10.3 (Bulter University, Indianapolis, IN). Differences between the means of dependent and independent groups were determined using paired *t*-test and unpaired *t*-test, respectively. Significant differences were assumed at *p* values less than 0.05.

Results

Formulation of rosemary oil in water nano-emulsion (REO/NE)

In this study, different fractions of the hydrophilic phase (distilled water), lipophilic phase (REO) and the mixture of surfactant and co-surfactant (tween 80 and span 20) at a ratio of 2:1, were used to determine the proportion of the constituents that resulted in one phase of the REO/NE product. Figure 1A–D show the three-, two- and bi-continuous phase emulsions produced at different proportions of the constituents. As displayed in Figure 1F, a clear one-phase REO/NE was obtained when 1.78% of REO was mixed with 92.8% of water in the presence of 5.41% of the mixture of tween 80 and span 20. Figure 2F shows the graph of turbidity of the resultant REO/NE at different heating temperatures. Turbidity was maintained from 25 to 60 °C, but it was markedly increased upon heating the system from 65 to 75 °C.

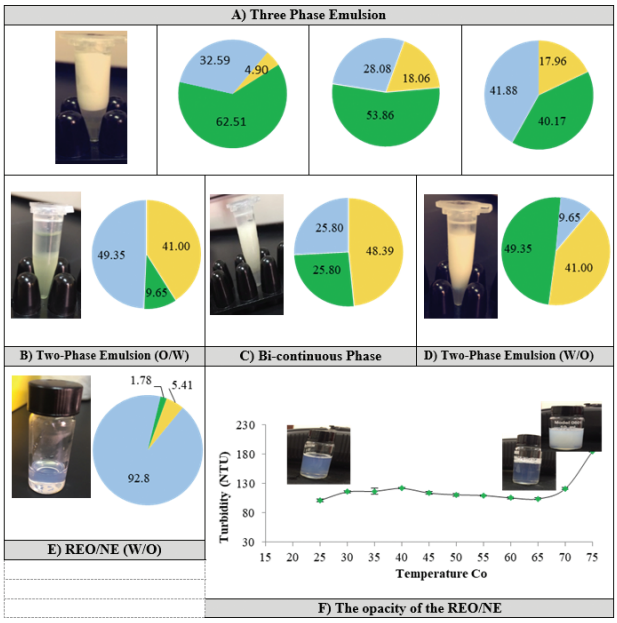

Figure 1. Pie charts showing three phases, two phases and one phase, based on the proportions of the constituents. **A**–**D** show three, two and bi-continuous phase emulsions. **E**: One phase of rosemary oil in water nano-emulsion (REO/NE). The green, blue and yellow slices represent the rosemary oil, distilled water and the mixture (2:1) of tween 80 to span 20, respectively. **F**: Turbidity – temperature curve of the resultant one-phase REO/NE showing the changes in the opacity of the formula at different temperatures. Data are presented as mean ±SD (n = 3).

Physical characteristics of REO/NE and REO/NE+MC using Zetasizer

The physical properties of the formulations are presented in Figure 2. The size distribution curves revealed that the mean diameters of synthesized REO/NE and REO/NE+MC were 59.22 ± 1.14 nm and 71.43 ± 1.32 nm, respectively, while both had similar polydispersity index of 0.02. In terms of zeta potential, the negative magnitude of REO/NE resulted in no remarkable change in the droplet charge after combined with MC.

Effects of MC, REO/NE and their combination on the viability of MCF-7 cells and HeLa cells

The effect of various concentrations of REO/NE and MC on the growth of MCF-7 and HeLa cells, expressed as fractions of cells affected (Fa) for 24 h (based on MTT assay), are shown in Figure 3A, B. The data demonstrates that the fractions of growth inhibition of the HeLa cells were markedly increased when treated with either the selected concentrations of REO/NE or when subjected to < 1.98 µM MC

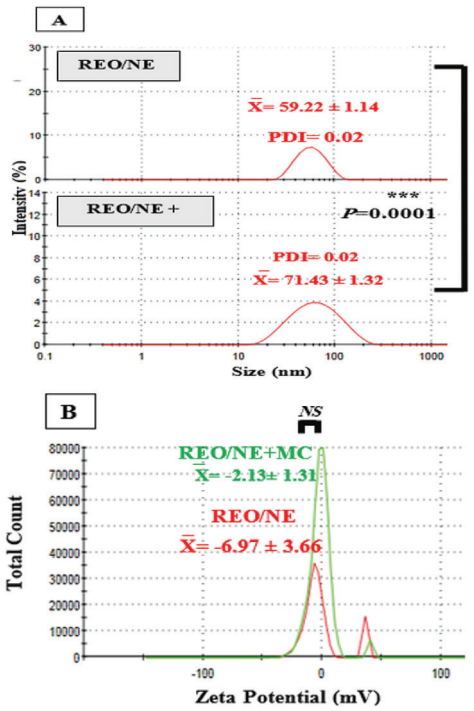

Figure 2. (**A**) Size and (**B**) zeta potential of REO/NE and REO/NE + MC, measured using DLS. The data are presented as mean ±SD (n = 3). The symbol NS indicates no significant difference; *** indicates significant differences between the formulations, ($p < 0.001$; paired sample *t*-test).

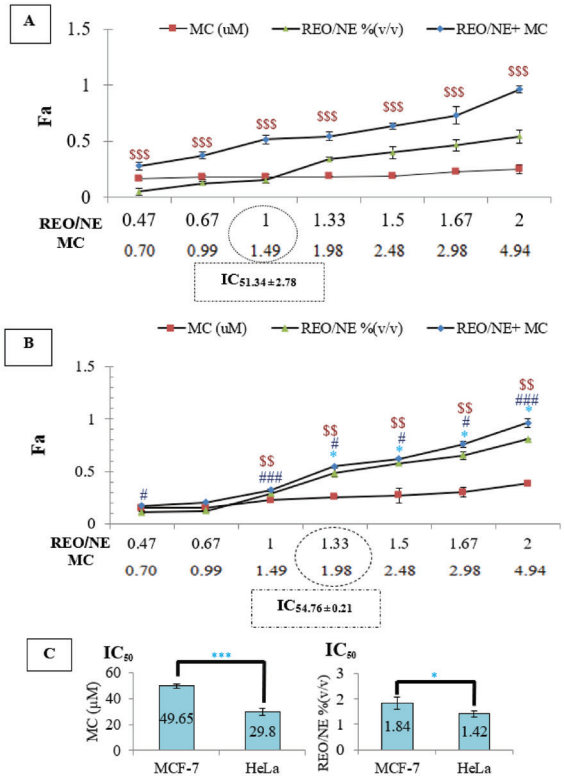

Figure 3. Inhibition of cell proliferation expressed as fraction affected (Fa) and assessed with MTT. Bar charts showing the Fa of (**A**) MCF-7 and (B) HeLa cells after 24 h of treatment with different drug concentrations. (**C**) IC_{50} of individual drug treatments. Data shown are presented as mean ±SD (n=3). The symbols $^{\#}$ and * indicate significant differences between MCF-7 and HeLa cells. $^{\$}$ indicates differences between MC and REO/NE + MC; $^{\#,*}P$ <0.05, $^{**}P$ <0.01, $^{\#\#\#,\ \$\$\$}P$ <0.001.

> Fa values of MCF-7 cells ($p < 0.05$). Figure 3C shows that REO/NE and MC exhibited dose-dependent cytotoxicity, with IC_{50} values of 1.83 ± 0.23% (v/v) and 49.65 ± 1.97 µM, respectively, on the MCF-7 cells, which were 1.30-fold and 1.66- fold, respectively, higher than those in HeLa cells. The half-maximal inhibitory concentration (IC_{50}) values of the individual drugs are shown in Figure 3C.

Furthermore, the MCF-7 and HeLa cells were treated with varying concentrations of the combination (REO/NE + MC) for 24 h, at levels that did not exceed the IC_{50} values of MC alone. The results in Figure 3A show 50% inhibition of cell growth when MCF-7 cells were treated with 1% (v/v) REO/NE + 1.49 µM of MC. In contrast, treatment of MCF-7 cells with 1% REO/NE and 1.49 µM led to 15% and 18% inhibitions of cell growth, respectively. Regarding HeLa cells, 49 and 26% inhibitions of cell growth resulted when they were subjected separately to 1.33% (v/v) REO/NE and 1.98 µM MC, while 50% inhibition of cell growth occurred when the two were combined (Fig. 3B).

Effect of combination of REO/NE and MC on MCF-7 and HeLa cells

Figure 4A shows the interactions between REO/NE and MC in MCF-7 and HeLa cells in dose-effect curves, which are represented by the *m* values obtained from their linearization with the median-effect plots (Fig. 4B) and summarized in Table 1. The result demonstrated that *m* values of the REO/NE dose-effect curves in both cell lines were similar ($p > 0.05$; m > 1), indicating steep curves, while the *m* value of MC was markedly lower in MCF-7 cells more than in HeLa cells ($p < 0.05$; m < 1), suggesting a shallower curve for MC in MCF-7 cells than in HeLa cells.

To determine whether the combination of REO/NE and MC produced higher cytotoxic effects on MCF-7 and HeLa cells than the predicted individual cytotoxicity, the Chou-Talalay method for non-constant ratio of REO/NE + MC combination was used to estimate the combination index (CI) through CompuSyn Software (Fig. 5). The results of Fa-CI plots revealed different patterns of interactions between REO/NE and MC in MCF-7 and HeLa cells. In particular, the CI values in MCF-7 cells increased in the direction of increasing the Fa values, with a value of 0.99 at Fa 0.54. However, a slight increase in the CI to 1.01 was observed when Fa increased to 0.7. At Fa 0.96, the CI value reached 0.6 and was similar to the CI at Fa 0.28. In contrast, for MCF-7 cells, CI values at Fa < 0.5 were above 1 and were slightly reduced to 1.1 at F 0.55. Thereafter, CI was decreased gradually to 0.43 at Fa 0.96.

Treatment with REO/NE + MC induced nuclear morphology change and apoptosis

To quantify the apoptotic effect of the individual and combined formulas of REO/NE and MC, the averages of

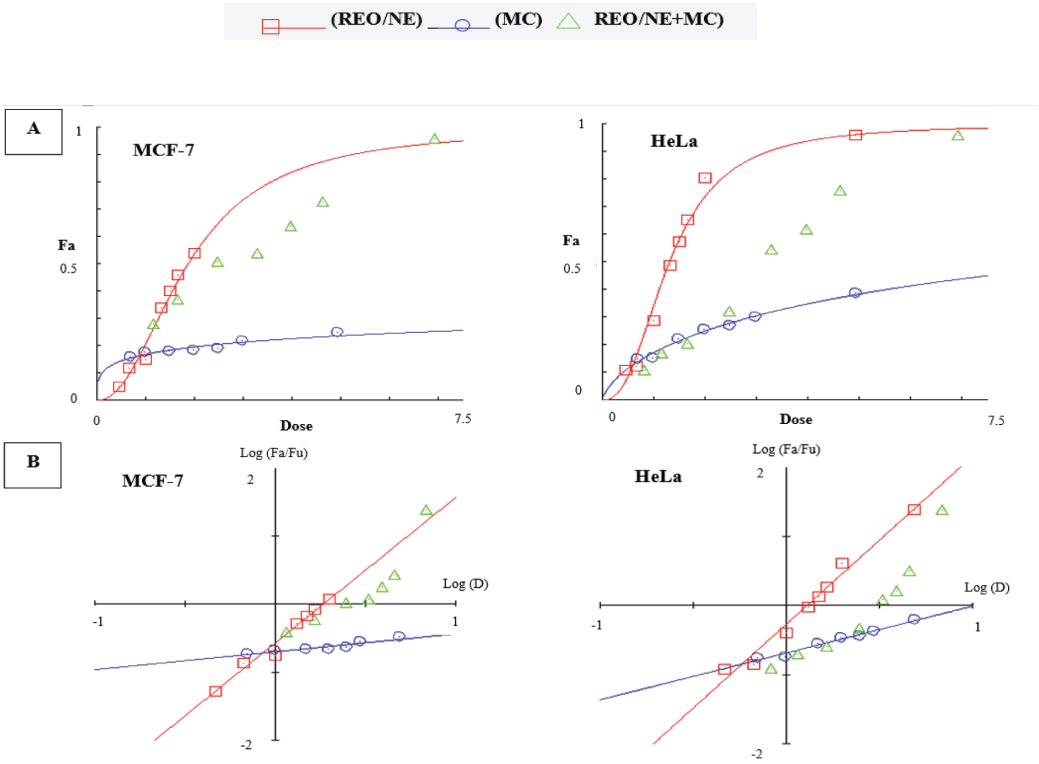

Figure 4. (**A**) Dose-Effect Curve, and (**B**) its linearization with Median-Effect Plots for effects of single and combination treatments with REO/NE and MC on MCF-7 and HeLa cells.

Table 1. Parameters of the dose-effect relationships for treatment with drug combinations of REO/NE with MC in MCF-7 and HeLa. Potency, shape and conformity of the median-effect plot are represented by Dm, m, and the linear correlation coefficient (r), respectively. Data shown are pooled results of a minimum of three independent experiments.

	Drug	Dm	m	r
MCF-7	REO/NE	1.86	2.14 ± 0.16	0.99
	MC	427.38	0.26 ± 0.04	0.93
HeLa	REO/NE	1.30	2.43 ± 0.15	0.99
	MC	10.00	0.68 ± 0.05	0.99

nuclear areas visualized via DAPI staining in the microscopic images of MCF-7 (Fig. 5A) and HeLa cells (Fig. 6A) are summarized in Figures 5B, 6B, respectively. Cells were treated for 24 h with 3 different concentrations of the formulas, chosen according to the results of MTT assay. At a concentration of 0.47% (v/v) REO/NE and 0.7 μM MC, treatment of MCF-7 cells with REO/NE produced markedly higher reduction in the nuclear areas, when compared with MC treatment MC ($p < 0.01$). In contrast, the nuclear areas of HeLa cells treated with MC were smaller than the corresponding areas of cells treated with REO/NE ($p < 0.05$). In the case of combination therapy, a higher decrease in the nuclear area of MCF-7 was observed with 0.7 μM MC combined with 0.47% (v/v) REO/NE, when compared the nuclear areas of MCF-7 due to individual drug treatments. When HeLa cells were treated with a similar concentration of the combination, the nuclear area appeared smaller than that of REO/NE-treated cells but was larger than that in MC-treated cells ($p < 0.01$).

However, the treatment of MCF-7 with 1% REO/NE (v/v) and HeLa cells with 1.33% (v/v) REO/NE produced the least nuclear areas, when compared to the cells treated with MC at doses of 1.48 μM and 1.98 μM MC only, or with the combined formulations. As the concentration of REO/NE was increased to 2% (v/v) and that of MC to 4.94 μM, MCF-7 cells exhibited more marked reductions in nuclear areas than when subjected to MC ($p < 0.01$). Treatment of MCF-7 cells with REO/NE combined with MC led to the least nuclear areas, relative to individual treatment ($p < 0.001$). On the other hand, Hela cells treated with 2% (v/v) REO/NE or 4.94 μM MC revealed similar nuclear areas ($p > 0.05$). However, smaller nuclei areas were produced with the combined formula ($p < 0.01$).

Discussion

Nano-delivery systems for transport of chemotherapeutic agents may minimize their severe side effects and the therapeutic doses. In this study, REO/NE produced with high-pressure homogenization technique, was used as a nano-carrier for the anticancer agent MC. The opacity of the REO/NE was determined from turbidity curve (Chuesiang et al. 2018). The opacity was maintained when the temperature was increased from 25 °C to 65 °C due to the small size of the nanodroplet diameter of REO/NE (59.22 ± 1.14 nm) and the narrow distribution of the mean droplet size (PDI = 0.02), which are known to influence the opacity property of the system (Mishra et al. 2014; Pagar

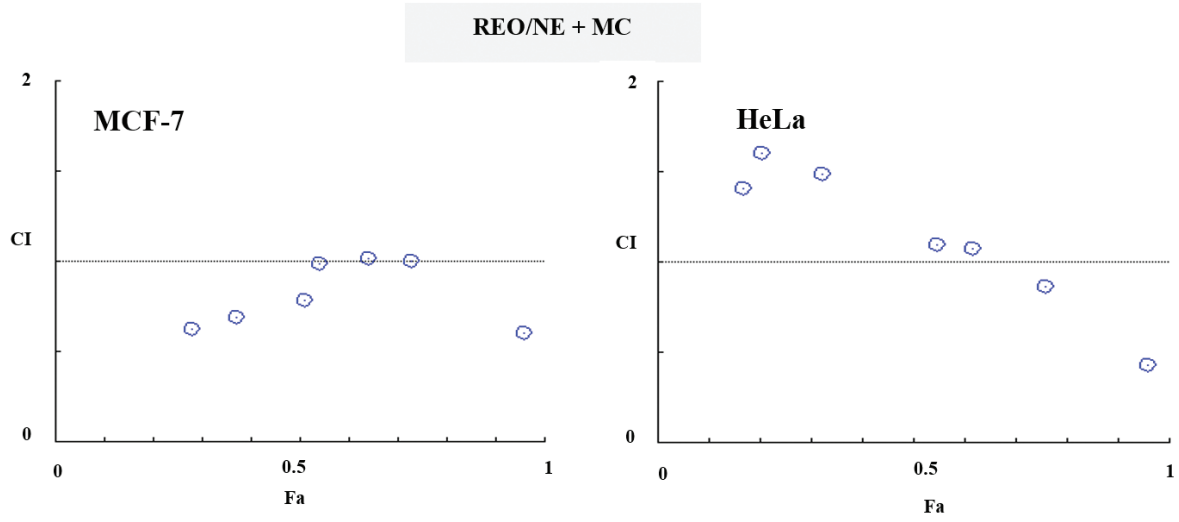

Figure 5. Fa-CI plots for the REO/NE + MC in MCF-7 and HeLa cell lines at different ratios. CI value less than, equal to, or greater than 1 indicates synergy, additivity, or antagonism, respectively. Affected fraction (Fa) indicates the fractional inhibition of the cells at which the CI value was calculated.

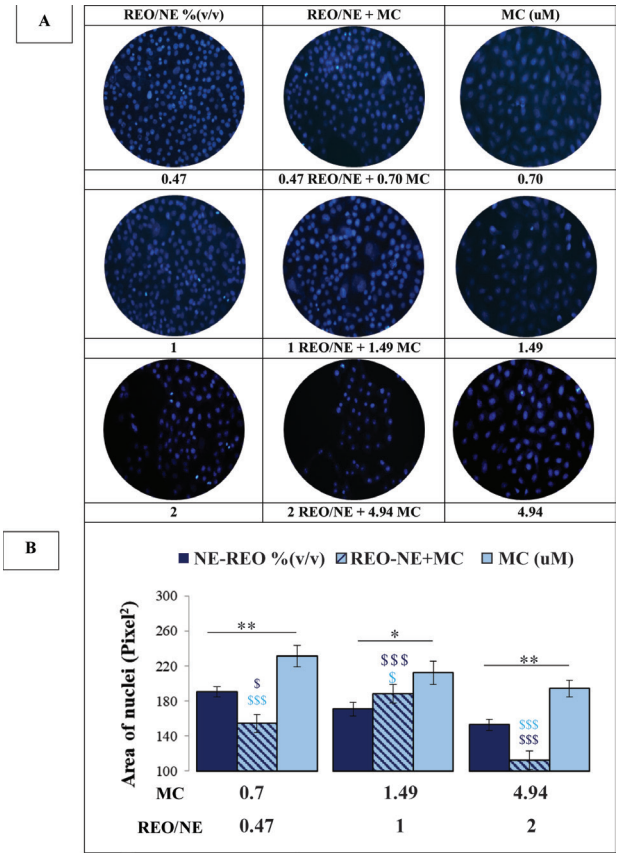

Figure 6. Fluorescence images (x400) of DAPI-stained MCF-7 cells treated with different formulations for 24 h. The treated cancer cells showed abnormalities in the nucleus ($^{\$,*}p$ <0.05, $^{**,\$\$}p$ <0.01, $^{***,\$\$\$}P$ <0.001). The symbol * indicates differences between MC and REO/NE; $^{\$}$ indicates differences between REO/NE + MC and each of the individual treatments. Data shown are results from a minimum of three independent experiments.

and Darekar 2019; Hien and Dao 2019). Moreover, REO has a low tendency for release in a hydrophilic environment due to its lipophilicity, resulting in increased connection with the lipophilic components in the NE droplets (Arabi et al. 2017). It is noteworthy that the REO/NE became less stable when the temperature of the solution was increased above 65 °C. This might be due to the presence of tween 80 and span 20, which tend to be more hydrophobic and poorly soluble in water as a result of having chains of polyethylene oxide moieties. Thus, the micelle enhanced the release of oil droplets to the hydrophilic phase, thereby forming a cloudy solution (McClements and Rao 2011; Sharma et al. 2013; Komaiko and McClements 2016).

Upon mixing MC with REO/NE, the droplet size of REO/NE+MC was markedly increased to 71.43 ± 1.32 nm without any significant change in the charge of the droplets, indicating that MC was incorporated inside the nanodroplets. Previous studies have reported that the diameter of a drug-incorporated nanocarrier is considerably larger than the diameter of the drug-free nanocarrier (Bahari and Hamishehkar 2016; Stella et al. 2018). With regard to the advantages of using REO/NE as a nanocarrier for MC, it was postulated that the combination may have synergistic or additive effects that would result in marked enhancement of the anti-cancer effects of MC. To achieve this, the growth inhibition concentrations of REO/NE, MC and their combined form against MCF-7 and Hela cells were determined using MTT assay. The results showed that REO/NE or MC caused higher marked dose-dependent growth inhibition of Hela cells than MCF-7 cells. Previous studies have shown that REO exerted antiproliferative effects against various cancer cells via inhibition of the signaling pathways for survival and proliferation (Wang et al. 2012; Valdes et al. 2013; Melusova et al. 2014; Valdes et al. 2016; Sujatha and Sirisha 2019). A recent study demonstrated high toxicity of liposomal carriers for REO against MCF7 cells due to the enhancement of REO delivery to the target cells (Salari and Salari 2019).

The synergistic effect of combination treatment on MCF-7 and HeLa cells was assessed using CalcuSyn software to

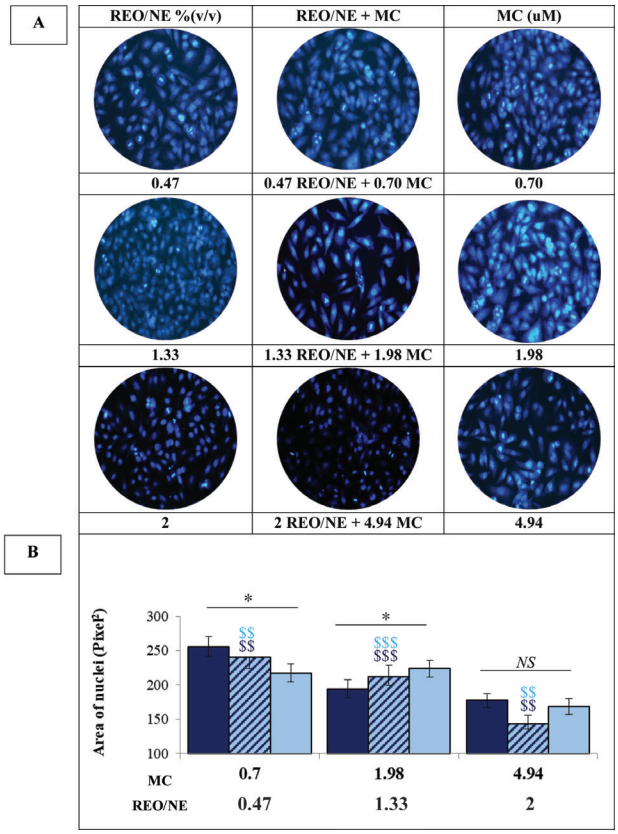

Figure 7. Fluorescence images (x400) of DAPI-stained HeLa cells treated with different formulations for 24 h. The treated cancer cells showed nuclear abnormalities. ($^{\$,*}P$ <0.05, $^{**,\$\$}p$ < 0.01, $^{***,\$\$\$}p$ <0.001, *NS* = not significant). The symbol * indicates differences between MC and REO/NE; $ indicates differences between REO/NE + MC and each of the individual treatments. Data shown are results of a minimum of three independent experiments.

determine the CI as described by Chou and Talalay. The Fa-CI plot revealed different patterns of interactions in the MCF-7 and Hela cells at low concentrations. In particular, synergistic antitumor activity was obtained via combination of 0.47% (v/v) REO/NE and 0.7 µM MC in MCF-7 cells (CI = 0.62, Fa= 0.28), while a clear evidence of antagonistic effect was demonstrated in HeLa cells (CI = 1.41, Fa= 0.17). At the IC_{50} for cell growth, there was a synergism between 1% (v/v) REO/NE and 1.49 µM MC on MCF-7 cells (CI = 0.79), while an additive effect of the combination was seen in HeLa cells after treatment with 1.33% (v/v) REO/NE and 1.98 µM MC (CI = 1). In fact, treatment of HeLa cells with 1.33% (v/v) and MCF-7 cells with 1% (v/v) REO/NE further decreased the IC_{50} value of the MC 15 times and 33.32 times, respectively. At the concentration of 2% (v/v) REO/NE and 4.94 µM MC, there was higher synergistic interaction of the combination between REO/NE and MC in HeLa cells (CI = 0.43, Fa = 0.96) than in MCF-7 cells (CI = 0.60, Fa = 0.96). These results confirm a synergistic anticancer effect on HeLa and MCF-7 cells at high concentrations of the REO/NE+MC.

To determine the cellular uptake mechanism of the drug formulas, the nuclei of treated cells were stained with DAPI and visualized under a fluorescence microscope. In MCF-7 cells, the reduction in the area of nuclei was higher in cells treated with REO/NE+MC at low doses (0.47% v/v REO/NE and 0.7 µM MC, and high doses (2% v/v REO/NE and 4.94 µM MC), and produced more apoptotic effects, when compared to the treatment with each drug alone. For HeLa cells, the least nuclear area resulted from treatment with high concentrations (2% v/v REO/NE + 4.94 µM MC), which indicates that REO/NE+MC induced higher apoptosis in HeLa than each of the individual drugs. The bioactive components of REO stimulate pathways responsible for apoptotic cell death in HepG2 cells (Melusova et al. 2014). Therefore, the increased apoptosis in cells treated with the combined formulation indicates that REO/NE would be an efficient carrier of MC since it enhanced MC delivery and its effect on the target cells through the induction of nuclear apoptosis (Salari and Salari 2019).

Conclusion

Rosemary oil nano-emulsion (REO/NE) could be a promising candidate for a synergistic effect with MC and greater anticancer efficiency through induction of nuclear apoptosis of MCF-7 and Hela cells. Based on these results, there is need for further investigations on the efficacy of combinations of REO/NE with MC or other standard chemotherapeutics in drug transport across a variety of human cancer cell lines.

References

Ahamad J, Uthirapathy S, Mohammed Ameen MS, Anwer ET (2019) Essential Oil Composition and Antidiabetic, Anticancer Activity of *Rosmarinus officinalis* L. leaves from Erbil (Iraq). Journal of Essential Oil Bearing Plants 22: 1544–1553. https://doi.org/10.1080/097206 0X.2019.1689179

Al-Otaibi WA, Alkhatib MH, Wali AN (2020) Protective role of nanoemulsion containing roman chamomile oil against mitomycin C-induced toxicity in Ehrlich ascites carcinoma bearing mice. Indian Journal of Biochemistry and Biophysics (IJBB) 57: 33–44.

Alkhatib MH, Al-Otaibi WA, Wali AN (2018) Antineoplastic activity of mitomycin C formulated in nanoemulsions-based essential oils on HeLa cervical cancer cells. Chemico-biological interactions 291: 72–80. https://doi.org/10.1016/j.cbi.2018.06.009

Almotwaa SM, Alkhatib MH, Alkreathy HM (2020) Incorporating ifosfamide into salvia oil-based nanoemulsion diminishes its nephrotoxicity in mice inoculated with tumor. Advanced Pharmaceutical Bulletin, 10. https://doi.org/10.15171/bi.2020.02

Arabi MH, Chabok H, Mirzapour A, Shafiee M (2017) Preparation of nanoliposomes containing *Rosmarinus officinalis* L. essential oil: A comparative study. Med. Commun. Biosci. Biotechnol. Res. Comm, 10, 103-108. https://doi.org/10.21786/bbrc/10.1/15

Arpagaus C (2019) PLA/PLGA nanoparticles prepared by nano spray drying. Journal of Pharmaceutical Investigation 49: 405–426. https://doi.org/10.1007/s40005-019-00441-3

Bahari LAS, Hamishehkar H (2016) The impact of variables on particle size of solid lipid nanoparticles and nanostructured lipid carriers; a

comparative literature review. Advanced pharmaceutical bulletin 6: e143. https://doi.org/10.15171/apb.2016.021

Bouyahya A, Belmehdi O, Benjouad A, El Hassani RA, Amzazi S, Dakka N, Bakri Y (2020) Pharmacological properties and mechanism insights of Moroccan anticancer medicinal plants: What are the next steps? Industrial Crops and Products 147: e112198. https://doi.org/10.1016/j.indcrop.2020.112198

Chevalier Y, Bolzinger MA (2019) Micelles and Nanoemulsions. Nanocosmetics. Springer. https://doi.org/10.1007/978-3-030-16573-4_4

Chraibi M, Farah A, Elamin O, Iraqui HM, Fikri-Benbrahim K (2020) Characterization, antioxidant, antimycobacterial, antimicrobial effcts of Moroccan rosemary essential oil, and its synergistic antimicrobial potential with carvacrol. Journal of Advanced Pharmaceutical Technology & Research 11: 1–25. https://doi.org/10.4103/japtr.JAPTR_74_19

Chuesiang P, Siripatrawan U, Sanguandeekul R, Mclandsborough L, Mcclements DJ (2018) Optimization of cinnamon oil nanoemulsions using phase inversion temperature method: Impact of oil phase composition and surfactant concentration. Journal of colloid and interface science 514: 208–216. https://doi.org/10.1016/j.jcis.2017.11.084

Elmowafy EM, Tiboni M, Soliman ME (2019) Biocompatibility, biodegradation and biomedical applications of poly(lactic acid)/poly(lactic-co-glycolic acid) micro and nanoparticles. Journal of Pharmaceutical Investigation 49: 347–380. https://doi.org/10.1007/s40005-019-00439-x

Erdem MG, Cinkilic N, Vatan O, Yilmaz D, Bagdas D, Bilaloglu R (2012) Genotoxic and anti-genotoxic effects of vanillic acid against mitomycin C-induced genomic damage in human lymphocytes in vitro. Asian Pacific Journal of Cancer Prevention 13: 4993–4998. https://doi.org/10.7314/APJCP.2012.13.10.4993

Gezici S, Sekeroglu N, Kijjoa A (2017) In vitro anticancer activity and antioxidant properties of essential oils from *Populus alba* L. and *Rosmarinus officinalis* L. from South Eastern Anatolia of Turkey. Indian Journal of Pharmaceutical Education and Research 51(3): S498–S503. https://doi.org/10.5530/ijper.51.3s.74

Guo M, Zhang L, He Q, Ali Arabi S, Zhao H, Chen W, Ye X, Liu D (2020) Synergistic antibacterial effects of ultrasound and thyme essential oils nanoemulsion against *Escherichia coli* O157:H7. Ultrasonics Sonochemistry: e04988. https://doi.org/10.1016/j.ultsonch.2020.104988

Hien LTM, Dao DTA (2019) Formation of nanoemulsion from black pepper essential oil by high speed homogenization method. Vietnam Journal of Chemistry 57: 352–356. https://doi.org/10.1002/vjch.201900033

Jo MJ, Jin IS, Park CW, Hwang BY, Chung YB, Kim JS, Shin DH (2020) Revolutionizing technologies of nanomicelles for combinatorial anticancer drug delivery. Archives of Pharmacal Research: 1–10. https://doi.org/10.1007/s12272-020-01215-4

Karami Z, Khoshkam M, Hamidi M (2019) Optimization of olive oil-based nanoemulsion preparation for intravenous drug delivery. Drug research 69: 256–264. https://doi.org/10.1055/a-0654-4867

Ko JC, Chen JC, Wang TJ, Zheng HY, Chen WC, Chang PY, Lin YW (2016) Astaxanthin down-regulates Rad51 expression via inactivation of AKT kinase to enhance mitomycin C-induced cytotoxicity in human non-small cell lung cancer cells. Biochemical pharmacology 105: 91–100. https://doi.org/10.1016/j.bcp.2016.02.016

Komaiko JS, Mcclements DJ (2016) Formation of food-grade nanoemulsions using low-energy preparation methods: A review of available methods. Comprehensive Reviews in Food Science and Food Safety 15: 331–352. https://doi.org/10.1111/1541-4337.12189

Kostková H, Etrych T, Říhová B, Kostka L, Starovoytová L, Kovář M, Ulbrich K (2013) HPMA Copolymer Conjugates of DOX and Mitomycin C for Combination Therapy: Physicochemical Characterization, Cytotoxic Effects, Combination Index Analysis, and Anti-Tumor Efficacy. Macromolecular bioscience 13: 1648–1660. https://doi.org/10.1002/mabi.201300288

Liu J, Bi J, Liu X, Zhang B, Wu X, Wellala CKD, Zhang B (2019) Effects of high pressure homogenization and addition of oil on the carotenoid bioaccessibility of carrot juice. Food & Function 10: 458–468. https://doi.org/10.1039/C8FO01925H

Mcclements D, Rao J (2011) Food-grade nanoemulsions: formulation, fabrication, properties, performance, biological fate, and potential toxicity. Critical reviews in food science and nutrition 51: 285–330. https://doi.org/10.1080/10408398.2011.559558

Melušová M, Jantová S, Horváthová E (2014) Carvacrol and rosemary oil at higher concentrations induce apoptosis in human hepatoma HepG2 cells. Interdisciplinary toxicology 7: 189–194. https://doi.org/10.2478/intox-2014-0027

Melusova M, Slamenova D, Kozics K, Jantova S, Horvathova E (2014) Carvacrol and rosemary essential oil manifest cytotoxic, DNA-protective and pro-apoptotic effect having no effect on DNA repair. Neoplasma 61: 690–699. https://doi.org/10.4149/neo_2014_084

Mishra RK, Soni G, Mishra R (2014) A review article: on nanoemulsion. World Journal of Pharmacy and Pharmaceutical Sciences 3: 258–274.

Murata S, Yamamoto H, Shimizu T, Naitoh H, Yamaguchi T, Kaida S, Takebayashi K, Miyake T, Tani T, Tani M (2018) 5-fluorouracil combined with cisplatin and mitomycin C as an optimized regimen for hyperthermic intraperitoneal chemotherapy in gastric cancer. Journal of surgical oncology 117: 671–677. https://doi.org/10.1002/jso.24906

Ozerhan IH, Urkan M, Meral UM, Unlu A, Ersöz N, Demirag F, Yagci G (2016) Comparison of the effects of Mitomycin-C and sodium hyaluronate/carboxymethylcellulose [NH/CMC](Seprafilm) on abdominal adhesions. Springerplus 5: e846. https://doi.org/10.1186/s40064-016-2359-2

Pagar KR, Darekar A (2019) Nanoemulsion: A new concept of Delivery System. Asian Journal of Research in Pharmaceutical Science 9: 39–46. https://doi.org/10.5958/2231-5659.2019.00006.7

Pinto A, Pocard M (2019) Hyperthermic intraperitoneal chemotherapy with cisplatin and mitomycin C for colorectal cancer peritoneal metastases: A systematic review of the literature. Pleura and peritoneum 4. https://doi.org/10.1515/pp-2019-0006

Rašković A, Milanović I, Pavlović N, Ćebović T, Vukmirović S, Mikov M (2014) Antioxidant activity of rosemary (*Rosmarinus officinalis* L.) essential oil and its hepatoprotective potential. BMC complementary and alternative medicine 14: e225. https://doi.org/10.1186/1472-6882-14-225

Salari S, Salari R (2019) Nanoliposomal system of rosemary essential oil made by specific human cell phospholipids and evaluation of its anti-cancer properties. Applied Nanoscience 9: 2085–2089. https://doi.org/10.1007/s13204-019-01009-1

Sharma N, Mishra S, Sharma S, Deshpande RD, Sharma RK (2013) Preparation and optimization of nanoemulsions for targeting drug delivery. International Journal of Drug Development & Research 5: 37–48.

Stella B, Peira E, Dianzani C, Gallarate M, Battaglia L, Gigliotti CL, Boggio E, Dianzani U, Dosio F (2018) Development and characteriza-

tion of solid lipid nanoparticles loaded with a highly active doxorubicin derivative. Nanomaterials 8: e110. https://doi.org/10.3390/nano8020110

Sujatha K, Sirisha KB (2019) Anti-cancer and Anti-oxidant activity of essential oils of *Rosmarinus officinalis*, Azadirachta indica, Syzygium aromaticum and Cymbopogon nardus. Journal of Pharmacognosy and Phytochemistry 8: 4493–4498.

Sutradhar KB, Amin ML (2013) Nanoemulsions: increasing possibilities in drug delivery. European Journal of Nanomedicine 5: 97–110. https://doi.org/10.1515/ejnm-2013-0001

Urkan M, Özerhan İH, Ünlu A, Can MF, Özturk E, Gunal A, Yağcı G (2017) Prevention of intraabdominal adhesions: an experimental study using mitomycin-C and 4% icodextrin. Balkan medical journal 34: e35. https://doi.org/10.4274/balkanmedj.2015.1359

Valdes A, García-Cañas V, Rocamora-Reverte L, Gómez-Martínez Á, Ferragut JA, Cifuentes A (2013) Effect of rosemary polyphenols on human colon cancer cells: transcriptomic profiling and functional enrichment analysis. Genes & nutrition 8: e43. https://doi.org/10.1007/s12263-012-0311-9

Valdes A, García-Cañas V, Kocak E, Simó C, Cifuentes A (2016) Foodomics study on the effects of extracellular production of hydrogen peroxide by rosemary polyphenols on the anti-proliferative activity of rosemary polyphenols against HT-29 cells. Electrophoresis 37: 1795–1804. https://doi.org/10.1002/elps.201600014

Wang W, Li N, Luo M, Zu Y, Efferth T (2012) Antibacterial activity and anticancer activity of *Rosmarinus officinalis* L. Essential oil compared to that of its main components. Molecules 17: 2704–2713. https://doi.org/10.3390/molecules17032704

Zhou Q, Ye M, Lu Y, Zhang H, Chen Q, Huang S, Su S (2015) Curcumin improves the tumoricidal effect of mitomycin C by suppressing ABCG2 expression in stem cell-like breast cancer cells. PLoS ONE 10(8): e0136694. https://doi.org/10.1371/journal.pone.0136694